Finite Element Analyzing the Influence of Cutting HT250 by Self-prepared Si₃N₄ Insert with Different Cutting Depth

Bo Wang*[a], Ning Cui[b], Yang Zhang[a]

[a]Zhuhai College of Jilin University, Zhuhai 519041, China
[b]Zhuhai City Polytechnic, Zhuhai 519090, China
wangbo00019@163.com

Based on the properties parameters of the self-prepared Si3N4 insert and HT250, the simulation models were created. Using these models, the results of cutting force, temperature and tool stress were availably obtained with different cutting depth. It was concluded by these results that the cutting force was linearly increasing with cutting depth increasing. The tool temperature was minimum at a_p=0.5mm. The stress-effective of tool was also linearly increasing along with cutting depth increasing. The cutting depth heavily influenced the cutting performance of Si3N4 ceramic.

1. Introduction

Si3N4 ceramic has been widely used in cutting tool material, due to its good mechanical properties at high temperatures, superior thermal shock resistance, and wear and corrosion resistance (Jiang et al., 2015). Before applied as cutting tools, the properties of developed Si3N4 ceramics must be test. Metal cutting process is a very complicated nonlinear problem (Lei et al., 1999). However, the finite element simulation could acquire the required accuracy data access to the real cutting experiment and the intuitive simulation image, predict the cutting properties of cutting tool and optimize cutting tool geometric parameters and cutting technology parameters (Liu et al, 1999; Li et al., 2002; Saffar et la., 2008; Chen et la., 2008). This method could avoid a large number of actual materials cutting experiment, and save time, manpower and material resources, when compared to the traditional cutting test.

In this paper, the cutting properties of cutting HT250 by Si3N4 insert were studied by finite element simulation (Liu et al., 2016). The numerical models (geometric models, mesh generation, material behavior model, Heat transfer model, etc.) were created, according to the properties of self-prepared Si3N4 insert and grey iron HT250. The simulation tests were carried out in deferent cutting condition (V_c=300m/min, a_p=0.3/0.5/0.8/1mm, f=0.15mm/rev). Based upon analyzing the results of cutting force, tool temperature and stress-effective after machining simulation, the influence of cutting HT250 by self-prepared Si3N4 ceramic was predict with different cutting depth. The cutting force was linearly increasing along with cutting depth increasing. The tool temperature was minimum at a_p=0.5. The stress-effective of tool was also linearly increasing with cutting depth increasing. Therefore, cutting depth heavily influenced the cutting performance of Si3N4 ceramics.

2. Preparing Si3N4 ceramic insert (Jiang, 2016)

Si3N4 ceramic was prepared in prophase study. The raw materials used in this study were consisted of α-Si3N4 powder, La2O3, Yb2O3 and MgO. The starting powder mixtures were ball milled for 24 h in ethanol using Si3N4 balls. After drying, the powder was gently grounded and passed through a 100 mesh sieve. The mixed powder was performed on graphite die with specific tolerance between graphite punch and die. The Si3N4 sample was prepared by Hot Pressing Sintering at 1800°C. Finally, the sample was made into Si3N4 inserts. The properties of Si3N4 inserts were listed in table 1.

Table 1: Properties of Si3N4 ceramic insert

Bending strength (MPa)	HV hardness (GPa)	Fracture toughness (MPa·m$^{1/2}$)	Poisson's ratio	Yong's modulus 10^3 Mpa	Heat conductivity (W/(m·K))	Heat capacity (J/(kg·K))
905	14.3	9.02	0.25	310	31	550

3. Finite element modeling

The Lagrangian formulation was adopted as the numerical approach in this work, which has been used to investigate the effect of machining parameters on residual stresses distribution. The Lagrangian formulation effectively analyzed the effect of cutting depth (Lin et al., 2000; Outerito et al., 2006; Salio et al., 2006).

3.1 Geometries and mesh generation

Some simplified geometric models were provided in Deform software. The geometric models of Si3N4 insert and HT250 workpiece were respectively created as CNMA432 type and strip body. Then, the workpiece and insert were meshed with, respectively, 61351 and 26994 isoparametric quadrilateral elements. In order to improve the accuracy of analysis, the tool nose geometry mesh was generated with element size ratio of 7. The mesh generations of Si3N4 insert and HT250 workpiece were respectively shown a and b in Figure 1.
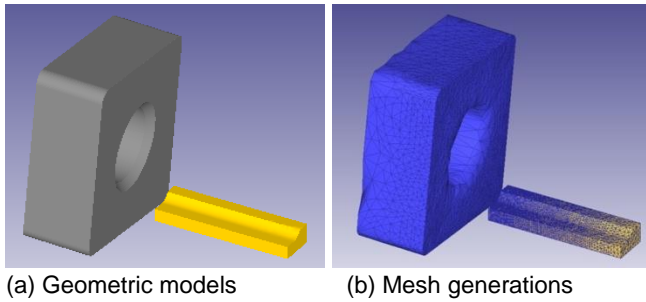

(a) Geometric models   (b) Mesh generations

Figure 1: Geometries and mesh generation

3.2 Material behavior modeling

(1) Workpiece material behavior modeling
The constitutive law proposed by Johnson and Cook (Outeiro et al., 2006) provides a good description of material behavior subjected to large strains, high strain-rates and thermal softening (Pedro and Ozel, 2010). The Johnson-Cook modeling, available in Deform software, is used in the simulation process. The law is described by Eq.1. The material used in this study is the grey iron HT250. The elastic and thermos-mechanical properties of HT250 are shown in Table 2.

$$\overline{\sigma} = [A + B(\overline{\varepsilon})^n] \left[1 + C \ln\left(\frac{\dot{\overline{\varepsilon}}}{\dot{\overline{\varepsilon}_0}}\right)\right] \left[1 - \left(\frac{T - T_{room}}{T_{melt} - T_{room}}\right)^m\right] \tag{1}$$

In Eq.1, σ is the material flow stress, $\overline{\varepsilon}$ is the equivalent plastic strain, $\dot{\overline{\varepsilon}_0}$ is the reference plastic strain rate, $\dot{\overline{\varepsilon}}$ is the plastic strain rate, T_{room} and T_{melt} are respectively the room and the melting temperatures. The coefficients (A, B C, n and m), listed in Table 3, are obtained from tensile curves using a fitting program [13].

Table 2: Elastic and thermal properties parameters of HT250

Density (Kg/m^3)	Poisson's ratio	Yong's modulus 10^3 Mpa	Heat conductivity (W/(m·K))	Thermal expansion (10^{-6}/°C)
7190	0.26	126	100°C 49.1 200°C 48.1 300°C 47.1 400°C 46.1 500°C 45.1	−100~20°C 10.0 20~200°C 11.0 200~400°C 12.5

Table 3: HT250 material constants for J-C model

A	B	C	n	m	T_{room}	T_{melt}	$\dot{\overline{\varepsilon}}_0$	$\dot{\overline{\varepsilon}}$
573	380	0.034	0.17	0.12	20	1250	1	1

(2) Insert material behavior modeling

In materials database of Deform software, the Al2O3 ceramic is defined by the Power Law, shown below Eq.2. In this study, Si3N4 ceramic was also defined by the Power law.

$$\overline{\sigma} = c \times \overline{\varepsilon}^n \times \dot{\overline{\varepsilon}}^m + y \qquad (2)$$

In Eq.2, $\overline{\sigma}$ is Flow stress, $\overline{\varepsilon}$ is effective plastic strain, $\dot{\overline{\varepsilon}}$ is effective strain rate, c is material constant, n is strain exponent, m is Strain rate exponent, y is initial yield value. The Si3N4 ceramic properties are shown in Table 1.

3.3 Contact and friction modeling

Zorev (Zorev, 1963) proposed the most realistic description of normal and frictional stress distribution at tool-chip interface, as shown in Figure 2. The author assumed that the tool-chip interface was subdivided into two zones (Moussa et al., 2012): sticking zone and sliding zone. In the sticking zone ($x \leq l_p$), the shear stress reach the saturation values τ_{max}. In the sliding zone ($l_p \leq x \leq l_c$), the frictional shear stress does not reach the saturation values τ_{max}. The frictional stress can be expressed as Eq3. In Eq.3, $\mu = 0.45$ (Xing and Hong, 1988).

$$\begin{cases} \tau_f = \mu \times \sigma_n \ if \ \mu \times \sigma_n < \tau_{max} \ (Sliding) \\ \tau_f = \tau_{max} \ if \ \mu \times \sigma_n \geq \tau_{max} \ (Sticking) \end{cases} \qquad (3)$$
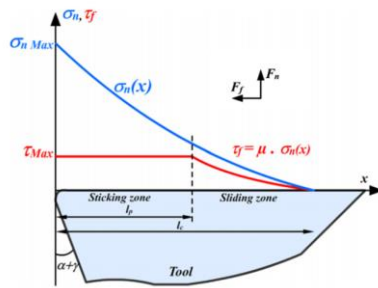

Figure 2: Normal and frictional stress distributions at tool–chip interface (Huang et al., 2005)

3.4 Heat transfer modeling

In machining, the temperature increases in cutting zone results from material plastic deformation and friction at tool-workpiece interface. Most of the heat is taken away by chip, parts of the heat is transferred into the air. In order to improve the accuracy of analysis, the heat transferred into air is expressed as Eq.4 (Ren et al., 2014).

$$Q_h = h \times (T_w - T_0) \qquad (4)$$

In Eq.4, $h = 0.02$ is convection coefficient, T_w is the surface temperature of insert and workpiece, $T_0 = 20°C$ is environment temperature (Xing and Hong, 1988).

4. Finite element simulation and discussions

After finite element modeling, the simulation tests were carried out in different cutting condition. The cutting parameters were listed in Table 4. The number of simulation steps parameter defined 500. Figure 4 was the images of simulation processes. Cutting force, stress, temperature field and stress field are the main analysis parameters for confirming cutting performance, analyzed after simulation.

Table 4: Cutting parameters

Cutting speed V_c (m/min)	Depth of cut a_p (mm)	Feed rate f (mm/rev)
300	0.3/0.5/0.8/1	0.15

4.1 Cutting force analysis

Cutting force is the main analysis parameters, related to cutting heat generation, tool wear, machining accuracy. Figure 3 showed the simulation results of the main cutting force, which gradually rise from zero up to maximum, stabilized within the particular range finally. The max main cutting forces in different cutting speeds (a_p=0.3, 0.5, 0.8, 1mm) were respectively 355N, 529N, 1022N, 1301N. The Relationship between the main cutting force and speed was shown in Figure 4. The cutting force was linearly increasing along with cutting depth increasing.
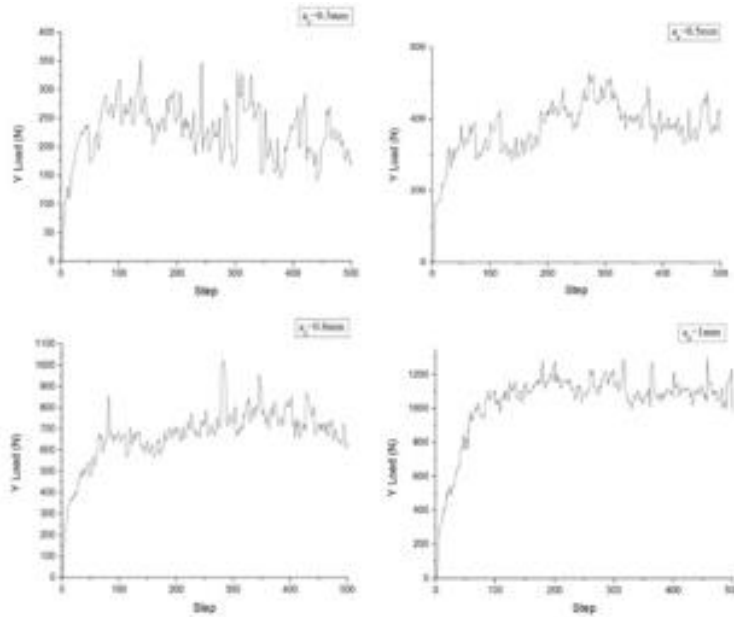

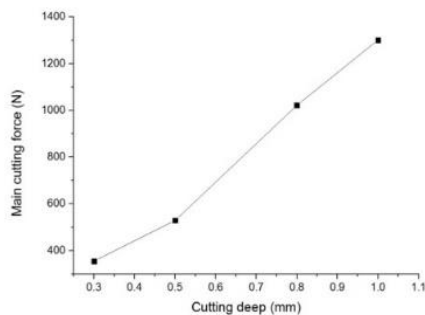*Figure 3: Results of the main cutting force*

Figure 4: Relationship between cutting force and cutting depth

4.2 Temperature field analysis

Heat generation is mainly caused by metal deformation in cutting process. The temperature values in different cutting speed were shown in Figure 5. The highest tool temperature in different cutting depth (a_p=0.3, 0.5, 0.8, 1mm) were respectively 24.4, 23.8, 30.9, 32.2°C, focused on tool nose. Figure 6 showed the relationship of tool temperature and cutting speed. The tool temperature was lowest in a_p=0.5mm. When cutting depth was beyond to 0.8, the tool temperature was observably rising. This was caused by metal deformation became severer as cutting depth increase in simulation process.
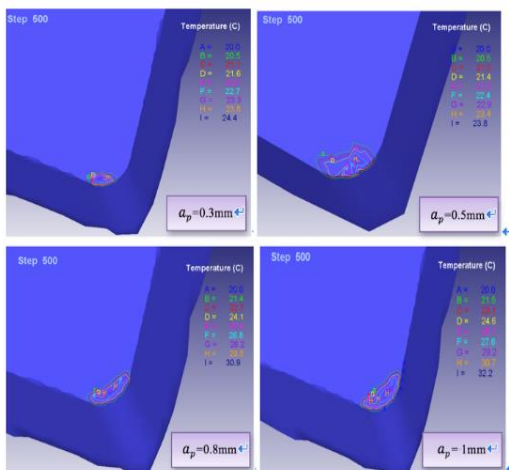
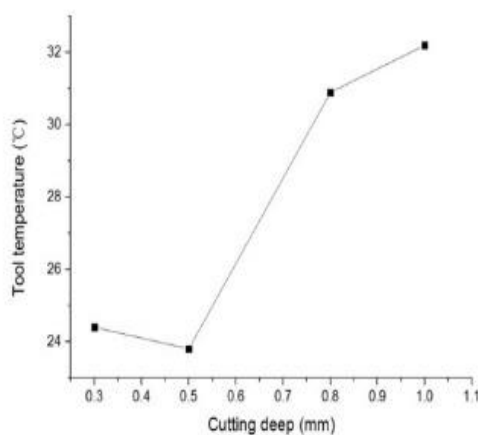*Figure 5: Temperature fields results of tool*

Figure 6: Relationship between tool temp and cutting depth

4.3 Tool stress-effective analysis

Tool stress-effective mainly reflects the internal stress distribution of tool influenced by cutting force, can quickly determine the dangerous area of tool in cutting process, effectively predict tool failure mode. Figure 7 showed respectively the tool stress-effective in different cutting depth (a_p=0.3, 0.5, 0.8, 1mm). Tool stress-effective was worse at tool nose than other area, which indicated the tool nose appeared wear firstly. The relationship between stress-effective and cutting speed was shown in Figure 8. With the cutting speed increasing, tool stress-effective was increasing linearly. However, the stress-effective in a_p=1mm declined trend, due to Si3N4 ceramics at tool nose had been occurred failure.
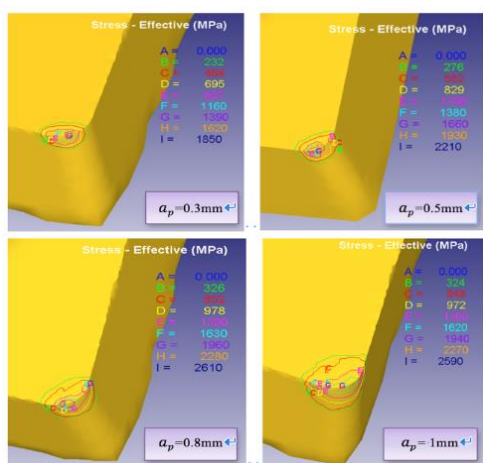

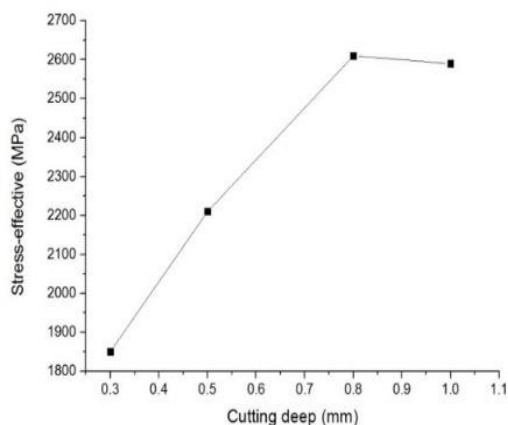*Figure 7: Stress-effective results of tool*

Figure 8: Relationship between stress-effective and cutting depth

5. Conclusions

In this paper, the cutting HT250 process by self-prepared Si3N4 ceramic insert was simulated in different cutting depth. Depended on analyzing the results of cutting force, tool temperature and stress-effective after machining simulation, the cutting properties of self-prepared Si3N4 insert were predict. It was concluded by the simulation results:

(1) The cutting force was increasing linearly along with cutting depth increasing.

(2) The tool temperature was lowest in a_p=0.5mm. When cutting depth was beyond to 0.8mm, the tool temperature was observably rising.

(3) With the cutting speed increasing, tool stress-effective was increasing linearly.

(4) The cutting depth heavily influenced the cutting performance of Si3N4 ceramic. The wear at tool nose became observably more serious with cutting depth increasing.

Acknowledgements

Reference

Chen W., Li W., Liu N., 2008, Performance of Ti(C,N)-based cermets cutter and simulation technique of cutting process, International Journal of Machine Tools and Manufacture, 197(1-3), 36-42, DOI: 10.1016/j.jmatprotec.2007.06.015.

Huang J., Shivpuri R., Cheng X., Bedekar V., Matsumoto Y., Hashimoto F., Watkins T.R., 2005, Effect of feed rate, workpiece hardness and cutting edge on subsurface residual stress in the hard turning of bearing steel using chamfer-hone cutting edge geometry, Mater Sci Eng, 394, 238-48. DOI: 10.1016/j.msea.2004.11.011.

Jiang Q., 2016, Studies on Preparation, Microstructure and Properties of Silicon Nitride with Ternary Sintering Additives, the PhD Thesis of Guangdong University of Technology, 41-61, In Chinese. DOI: 10.7666/d.Y2953208.

Jiang Q., Liu J., Guo W., 2015, A Novel Hot Pressing Flowing Sintering for Preparation of Texturing Ceramics, The American Ceramic Society, 98(9), 2696-2699. DOI: 10.1111/jace.13715.

Lei S., Shin Y., Incropera F., 1999, Thermo-mechanical modeling of orthogonal machining process by finite element simulation, International Journal of Machine Tools and Manufacture, 39(5), 731-750.

Li K., Gao X., Sutherland J.W., 2002, Finite element simulation of the orthogonal metal cutting process for qualitative understanding of the effects of crater wear on the chip formation process, Journal of Materials Processing Technology, 127(3), 309-324. DOI: 10.1016/S0924-0136(02)00281-9.

Lin Z., Lai W., Liu C., 2000, The study of ultra-precision machining and residual stress for NiP alloy with different cutting speeds and depth of cut, J Mater Process Technology, 97, 200-210, DOI: 10.1016/S0924-0136(99)00373-8.

Liu D., Yu X., Lou P., 1999, Finite element analysis of temperature distribution in orthogonal metal machining, Journal of Beijing Institute Technology, 8(4), 386-391.

Liu Y.M., Wang J., Ji W.F., Luo G.Q., 2016, Temperature field finite element analysis of the ultra-high temperature borehole inclinometer based on fog and its optimization design, Chemical Engineering Transactions, 51, 709-714, DOI: 10.3303/CET1651119.

Moussa N.B., Sidhom H., Braham C., 2012, Numerical and experimental analysis of residual stress and plastic strain distributions in machined stainless steel, International Journal of Mechanical Sciences, 64, 82-93, DOI: 10.1016/j.ijmecsci.2012.07.011.

Outeiro J.C., Umbrello D., M'Saoubi R., 2006, Experimental and numerical modeling of the residual stresses induced in orthogonal cutting of AISI 316L steel, Int J Mach Tools Manuf, 46, 1786-94. DOI: 10.1016/j.ijmachtools.2005.11.013.

Pedro J.A., Ozel T., 2010, Investigations on the effects of friction modeling in finite element simulation of machining, International Journal of Mechanical Sciences, 52, 31-42. DOI: 10.1016/j.ijmecsci.2009.10.001

Ren J., Hu X., Wang M., Yan S., Wu B., 2014, Comparison the Cutting Performance of 300M Ultra High Strength Steel Based on DEFORM-3D, Modular Machine Tool and Automatic Manufacturing Technique, 12, 34-47.

Saffar J.R., Razafar M.R., Zarei O., 2008, Simulation of three -dimension cutting force and tool deflection in the end milling operation based on finite element method, Simulation Modelling Practice Theory, 16(10), 1677-1688.

Salio M., Berruti T., De Poli G., 2006, Prediction of residual stress distribution after turning in turbine disks. Int J Mech Sci, 48, 976-84, DOI: 10.1016/j.ijmecsci.2006.03.009.

Zorev N.N., 1963, Inter-relationship between shear processes occurring along tool face and shear plane in metal cutting, International research in production engineering, New York, ASME, 42-49.